Oxygen Ion Drift-Induced Complementary Resistive Switching in Homo $TiO_x/TiO_y/TiO_x$ and Hetero $TiO_x/TiON/TiO_x$ Triple Multilayer Frameworks

*Yoon Cheol Bae, Ah Rahm Lee, Ja Bin Lee, Ja Hyun Koo, Kyung Cheol Kwon, Jea Gun Park, Hyun Sik Im, and Jin Pyo Hong**

Developing a means by which to compete with commonly used Si-based memory devices represents an important challenge for the realization of future three-dimensionally stacked crossbar-array memory devices with multifunctionality. Therefore, oxide-based resistance switching memory (ReRAM), with its associated phenomena of oxygen ion drifts under a bias, is becoming increasingly important for use in nanoscalable crossbar arrays with an ideal memory cell size due to its simple metal–insulator–metal structure and low switching current of 10–100 μA. However, in a crossbar array geometry, one single memory element defined by the cross-point of word and bit lines is highly susceptible to unintended leakage current due to parasitic paths around neighboring cells when no selective devices such as diodes or transistors are used. Therefore, the effective complementary resistive switching (CRS) features in all Ti-oxide-based triple layered homo $Pt/TiO_x/TiO_y/TiO_x/Pt$ and hetero $Pt/TiO_x/TiON/TiO_x/Pt$ geometries as alternative resistive switching matrices are reported. The possible resistive switching nature of the novel triple matrices is also discussed together with their electrical and structural properties. The ability to eliminate both an external resistor for efficient CRS operation and a metallic Pt middle electrode for further cost-effective scalability will accelerate progress toward the realization of cross-bar ReRAM in this framework.

1. Introduction

Future non-volatile memories (NVMs) should facilitate the continuing miniaturization of data memory storage, enable ultralow power operation, require a low switching current, and exhibit high endurance/retention performance. Among the recently considered NVMs, such as phase change memory, polymer memory, spin transfer torque magnetic memory, and resistance switching memory (ReRAM), ReRAM is becoming increasingly important due to its high-density integration, long retention time, small size, and fast switching speed.[1–4] Because of its simple metal–insulator–metal (MIM) structure, ReRAM is highly promising for use in nanoscalable crossbar arrays with an ideal $4F^2$ (F = minimum feature size;[5]) memory cell size.[5] A two-terminal passive array of nanoscale crossbar frameworks consists of a set of electrically resistive switching elements (called memristive elements) for the ReRAM device sandwiched between perpendicular bottom and parallel top electrodes as possible resistive switching building blocks.[6–8] However, one single element defined by the cross-point of word (top) and bit (bottom) lines is highly susceptible to unintended leakage current due to parasitic paths around neighboring cells. As such, the integration of a selection device, such as a diode or transistor, is required at each node.[9] The use of a selection device in practical memory devices has been hindered and much effort has been dedicated toward the development of

Y. C. Bae, A. R. Lee, K. C. Kwon, Prof. J. P. Hong
Division of Nanoscale Semiconductor Engineering
Hanyang University
Seoul, 133-791, South Korea
E-mail: jphong@hanyang.ac.kr

J. B. Lee, J. H. Koo, Prof. J. P. Hong
The Research Institute for Natural Sciences
Novel Founctional Materials and Devices Lab.,
Department of Physics
Hanyang University
Seoul, 133-791, South Korea

K. C. Kwon, Prof. J. G. Park
National Program Center for Tera-bit-level
Nonvolatile Memory Development
Hanyang University
Seoul 133-791, South Korea

Prof. J. G. Park
Department of Electronic Engineering
Hanyang University
Seoul 133-791, South Korea

Prof. H. S. Im
Department of Semiconductor Science
Dongguk University
Seoul 100-715, South Korea

DOI: 10.1002/adfm.201102362

both ReRAM crossbar arrays on a silicon-based complementary metal-oxide semiconductor (CMOS) transistor and rectifying diodes.[10–14] Therefore, control and manipulation of multiple sneak path problems is one of the key approaches that have been employed in the development of high density crossbar ReRAM devices.

To implement ReRAM in a nanoscalable crossbar array, the complimentary resistive switching (CRS) concept that addresses the sneak path problem without the use of a selection device was initially tested. Waser et al. proposed a conductive bridge memory (CBM) device based on two bipolar resistive switching elements (memristive elements 1 and 2) connected anti-serially.[15,16] The superimposed current–voltage (*I–V*) properties of the two bipolar switching elements confirmed CRS behavior in the anti-serially stacked CBM device, suggesting the possibility of overcoming the sneak path problem without utilizing selection devices. The CBM device basically employed a middle conductive Pt electrode between two memristive elements, and the non-symmetric SET and RESET threshold voltages for CRS required an additional resistor in series that was integrated with the CRS device for a functional memory margin.[17] Recently, Lee's group reported on a fast and highly scalable NVM in the form of an asymmetric 30-nm-scale Ta_2O_{5-x}/TaO_{2-x} bilayer structure, thus demonstrating a successful working crossbar device.[18] An additional metal Pt electrode in the middle region of this bilayer structure was used for CRS. Given the above findings, practical questions remain regarding fabrication costs, and so on. A particularly interesting geometry for CRS was employed in this work to induce a high voltage reset process after the set process during CRS and allow for cost-effective scalability in future 3D stacked structures.

Here, we demonstrate the CRS phenomena of simple homo $TiO_x/TiO_y/TiO_x$ and hetero $TiO_x/TiON/TiO_x$ triple multilayer geometries as alternative resistive switching matrices. Each matrix is typically based on anti-serially combined bipolar switching elements 1 and 2. Bipolar switching element 1 (called memristor 1) consists of a top TiO_x (oxygen ion rich region) layer and a middle TiO_y or TiON (oxygen ion deficient region) layer, while bipolar switching element 2 (called memristor 2) is composed of the same materials in reverse order. The two switching elements are merged anti-serially for CRS. In particular, the need for an external resistor for CRS and an additional middle Pt electrode for future cost-effective scalability is eliminated. We analyze the structural and electrical properties of the anti-serially stacked matrices at room temperature (RT). In addition, we study the function of movable oxygen content so as to confirm the controllable memory features in our simple matrices under a bias and examine a possible resistive switching model emphasizing the interfacial roles between oxide layers.

A more detailed description of the fabrication process for the homo and hetero triple multilayer matrices is given in the Experimental Section.

2. Results and Discussion

Briefly, all CRS cells were first prepared on a bottom Pt electrode. In order to evaluate the role of different oxygen content in CRS, two test devices with different oxygen content in the top and bottom TiO_x layers were fabricated. In our work, two oxygen partial pressures were intentionally chosen so as to produce different oxygen content in the top and bottom TiO_x layers. For the top and bottom TiO_x layers, the ratio of the oxygen partial pressure rate to the total working pressure was 40% for Sample A and 70% for Sample B. The middle TiO_y (0%) layer for Samples A and B was deposited in an Ar-only atmosphere. Therefore, the configuration of Sample A was TiO_x (40%)/TiO_y (0%)/TiO_x (40%), while that of Sample B was a TiO_x (70%)/TiO_y (0%)/TiO_x (70%). The top Pt electrode in both samples was a 100-nm-thick square (100 μm × 100 μm), as determined by a commercial photolithography and lift-off method that was used to define the junction area. The CRS structures did not have a middle conductive Pt electrode.

Shown in **Figure 1**a is the typical geometry for Sample A; all Ti-oxide layers have a thickness of 20 nm and the top and

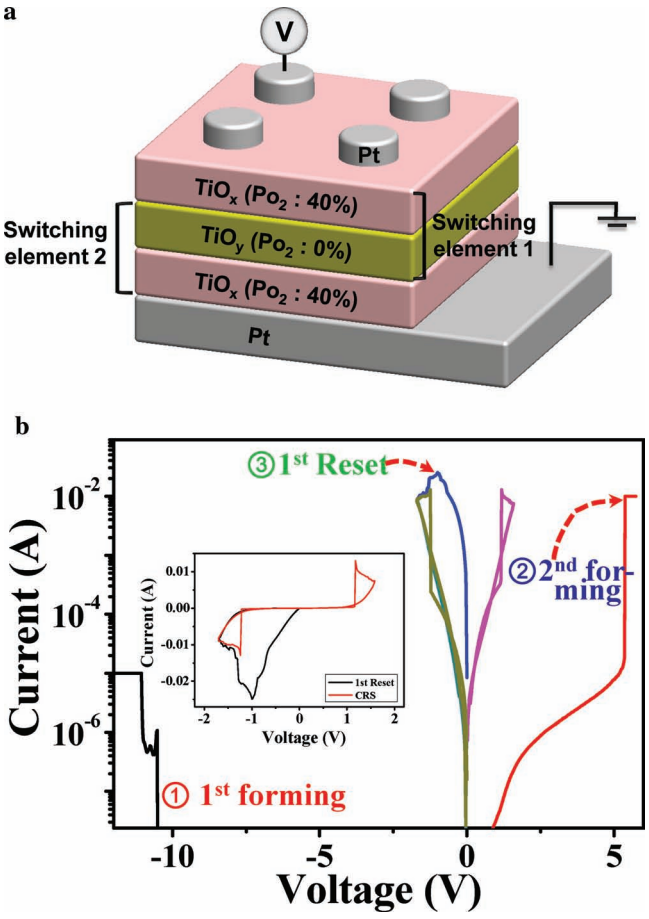

Figure 1. Geometry of the homo Pt/TiO_x/TiO_y/TiO_x/Pt memory cell and its electrical *I–V* characteristics. a) Schematic of a typical Ti-oxide based triple multilayer framework with an oxygen content of 40% in the top/bottom TiO_x and 0% in the middle TiO_y layers; the need for a middle metallic Pt electrode is eliminated. b) Electrical *I–V* characteristics of a Pt/TiO_x (40%, top)/TiO_y (0%, middle)/TiO_x (40%, bottom)/Pt memory cell for CRS. At first, the existence of the two-step forming process (black and red lines) is observed. Following the first electroforming step (black line), the memory cell is still in the OFF state (LRS/HRS) and thus, an opposite second electroforming step (red line) is required to allow the cell to switch to the ON state (LRS/HRS). A thorough analysis reveals that the voltage of the first forming process is double that of the second forming process. The inset of (b) shows the *I–V* characteristics on a linear scale; inhibited resistive switching regions are observed from –1.3 V to 1 V for CRS.

bottom TiO_x layers are designed to have different oxygen content with respect to the middle TiO_y layer. As shown in Figure 1b, a two-step electroforming process is required to induce electrical CRS *I–V* features in our configurations. In the initial state (as-grown state), the top and bottom TiO_x layers are in a high resistance state (HRS), which is related to the large amount of movable oxygen ions (O^{2-}), while the TiO_y layer stays in a low resistance state (LRS) due to the relatively low concentration of O^{2-} and high concentration of oxygen vacancies ($V_{\ddot{O}}$). Electrical characteristics of each single layer were tested with the top and bottom Pt electrodes in MIM structures. As expected, the single TiO_x layer displayed only unipolar resistive switching, while the other single TiO_y layer works like a resistor (Supporting Information Figure S1). Therefore, the fully stacked structure of Sample A initially remains in a HRS (top)/LRS (middle)/HRS(bottom) state and acts as a voltage divider under a bias. That is, memristor 1 is in a HRS/LRS state, while memristor 2 is in a LRS/HRS state. In addition, the top and bottom TiO_x layers, which have the same thickness, should possess the same resistance corresponding to an equal voltage drop under a bias. For CRS, if the first electroforming step (black line) is applied, memristor 1 or 2 will produce the total LRS state (i.e., LRS/LRS), while the other memristor will stay in the total HRS state (LRS/HRS). Thus, the CRS memory cell will remain in an OFF state. Therefore, the CRS cell requires an opposite second electroforming step (red line) for the CRS cell to switch to the ON state. With the application of a second electroforming voltage with the same polarity as that used in the first forming process, the CRS cell will only exhibit unipolar resistive switching (Supporting Infomation Figure S2). The polarity dependence of the forming process in bipolar resistive switching has previously been reported and is indirect evidence of an interface switching phenomena in bipolar resistive switching.[19] It should also be noted that the first and second forming processes take place at different voltages, as shown in Figure 1b. The voltage (–10.5 V) of the first forming process is almost double that of the second forming process (+5.2 V). In other words, the performance of the first positive forming process should allow one TiO_x layer of memristor 1 or 2 to switch to an LRS state, thus providing a reduction in the second forming voltage under an opposite voltage bias. Therefore, two forming processes are always required for CRS in our configuration. The expected superimposed *I–V* curve is shown in Figure 1b. The CRS behavior on a linear scale is illustrated in the inset of Figure 1b; exactly suppressed current regions are observed between –1.3 V and 1 V. The appearance of the first reset process in this figure will be explained later.

Two bipolar resistive switching elements, memristors 1 and 2, were connected anti-serially without a middle Pt electrode in order to study the CRS characteristics. The typical geometric configuration and *I–V* features of memristors 1 and 2 are shown in **Figure 2**a,b, respectively. In Figure 2c, the anti-serially connected triple multilayer of Sample A is displayed and its *I–V* features are analyzed. As shown in Figure 2a,b, typical Ti oxide-based bilayer homostructures gave rise to expected bipolar switching phenomena for switching elements 1 and 2. In previous work, it was suggested that switching elements 1 and 2 follow counter-clockwise (CCW) and clockwise (CW) resistive switching directions, respectively.[20] The nature of the bipolar

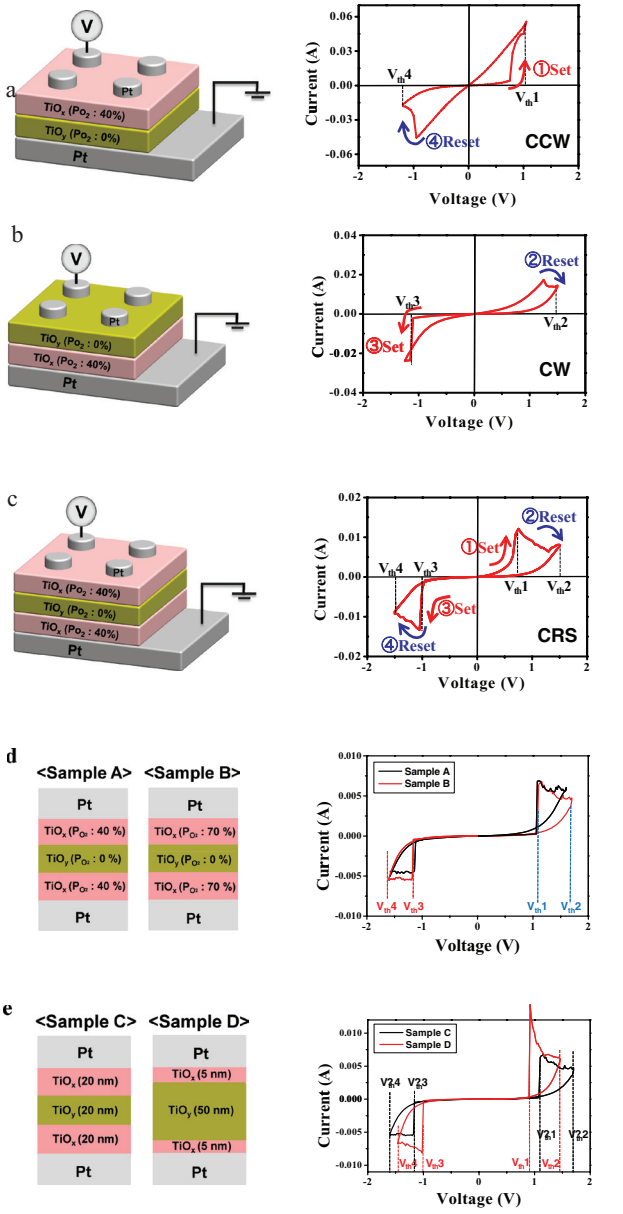

Figure 2. Sweep diagrams of bipolar and CRS phenomena on a linear scale. a) Schematic and *I–V* characteristics of bipolar switching element 1; switching element 1 switches to the LRS via a positive set process and to the HRS via a negative reset process. b) Schematic and *I–V* characteristics of bipolar switching element 2; switching element 2 switches to the LRS and HRS via a set/reset process opposite of that for element 1. CCW and CC denote the counter-clockwise and clockwise switching directions for switching elements 1 and 2, respectively. c) Typical Ti oxide-based structure and *I–V* characteristics of CRS, where bipolar switching elements 1 and 2 are anti-serially merged without the use of a middle Pt electrode. d) Oxygen content dependence of the CRS characteristics for Samples A and B; Sample B is designed to have more oxygen ions than sample A so as to provide a larger memory window in the CRS process. The measured *I–V* curve for Sample B clearly reveals a unique "butterfly" shape with a slightly large memory margin. e) Oxide thickness dependence of the CRS characteristics, as indicated in the *I–V* curves obtained for Samples C and D. As expected, the thinner top and bottom TiO_x layers in Sample D lead to a decrease in the operating threshold voltage. That is, a thinner TiO_x layer means a low voltage drop under bias, producing a corresponding lower threshold voltage for CRS.

resistive switching resulted from a combination of the filamentary conduction path and its redox reaction induced by the drift of oxygen ions at the interfaces in the bilayer TiO_x/TiO_y structure (Supporting Information Figure S3).[21] The butterfly *I–V* curve of the CRS cell with both set/reset processes in one polarity is shown in Figure 2c. For example, under a positive bias, switching element 1 has a set process (denoted as ① set) at threshold voltage 1 ($V_{th}1$), while switching element 2 has a reset process (denoted as ② reset) at threshold voltage 2 ($V_{th}2$). In contrast, under a negative bias, switching element 2 has a set process (denoted as ③ set) at threshold voltage 3 ($V_{th}3$) and switching element 1 has a reset process (denoted as ④ reset) at threshold voltage 4 ($V_{th}4$). These set and reset processes at one polarity are a consequence of the unique butterfly shape in the *I–V* curve of the CRS cell.

To further predict the effects of the movable oxygen ion content on the CRS characteristics, Samples A and B were compared. As mentioned above, the difference in the two samples lies in their oxygen ion content. As shown in Figure 2d, Sample A is composed of top and bottom TiO_x layers deposited at a 40% oxygen gas partial pressure, while Sample B contains top and bottom TiO_x layers grown at a 70% oxygen gas partial pressure. In our previous work, the stoichiometric amount of Ti and O atoms in TiO_x and TiO_y layers was confirmed via Rutherford backscattering spectrometry (RBS) measurements.[21] The TiO_y layer (0%) has a chemical composition of $TiO_{1.39}$, while TiO_x layers prepared within the 10–70% oxygen gas partial pressure range have chemical compositions in the range of $TiO_{1.50}$–$TiO_{1.90}$. In bipolar resistive switching, the memory window at current levels between the LRS and HRS exhibited a strong dependence on the oxygen content difference between the TiO_x and TiO_y layers (Supporting Information Figure S4).[21] Similarly, as shown in Figure 2d, the memory windows in the CRS cell reflect different behaviors for Samples A and B, although the threshold operating voltages ($V_{th}1,2,3,4$) for the two samples are similar. These findings are in good agreement with our previous results obtained with bilayer switching elements. The larger memory window in Sample B may be the consequence of a larger number of migrated oxygen ions and stronger set and reset processes during resistive switching when compared to those of Sample A.

To provide indirect evidence for intentional control of electrical features, the thickness dependence of the CRS characteristics was also investigated with two different specimens, Samples C and D; the results are presented in Figure 2e. The oxide thickness of Sample C was symmetric (i.e., 20 nm:20 nm:20 nm = 1:1:1) in a $TiO_x/TiO_y/TiO_x$ configuration, while Sample D possessed an asymmetric thickness ratio (5 nm:50 nm:5 nm = 1:10:1). As shown in Figure 2e, the set ($V_{th}1$, $V_{th}3$) and reset ($V_{th}2$, $V_{th}4$) voltages for Sample D are smaller than those for Sample C ($V'_{th}1,2,3,4$). In addition, a slightly larger memory window is observed in Sample D. On the basis of the nature of bipolar resistive switching in memristors 1 and 2, the thickness dependence of the CRS cell suggests that the thinner TiO_x layer in Sample D requires a small operating voltage for resistive switching due to its relatively low layer resistance. In addition, while the same bias is applied to Samples C and D, the effective bias of Sample D may allow for a larger number of migrated oxygen ions in the TiO_x layer. This would explain why Sample D exhibits small operating voltages and larger memory windows. We note that this rough finding supports the possibility of controlling a memory feature by varying the oxygen content or oxide thickness in a CRS cell. These characteristics were further validated via pulse mode measurements, where similar trends were observed (Supporting Information Figure S5).

To verify alternative CRS behavior in a different triple multilayer configuration, we also developed an anti-serially stacked hetero $TiO_x/TiON/TiO_x$ cell. The most significant aspect of this cell is the use of an oxy-nitride as a middle layer. This layer acts as an interfacial redox reaction region between the TiO_x/TiON and TiON/TiO_x for memristors 1 and 2. Shown in **Figure 3** are the geometric layout and electrical *I–V* characteristics of a hetero $Pt/TiO_x/TiON/TiO_x/Pt$ cell with top and bottom TiO_x layers with different thicknesses (t_1 = 5, 20, 30 nm) prepared under 70% oxygen gas partial pressure; the middle TiON layer in the structures had a thickness of 10 nm. As predicted earlier from the homo Ti oxide-based memory cell results, our hetero memory cells also exhibit typical butterfly *I–V* curves after a two-step electroforming process (data not shown). In our previous work (Supporting Information Figure S6), we suggested that the naturally formed TiON interfacial region in a TiO_x/TiN configuration may play a key role in bipolar resistive switching and reduce the operating current level in bipolar resistive switching.[22–24] Therefore, typical CCW and CW bipolar *I–V* curves for switching elements 1 and 2, together with the CRS phenomenon of the hetero $TiO_x/TiON/TiO_x$ cell are thoroughly explained in the Supporting Infomation (Figure S7).

In particular, we note that the CRS characteristics of a hetero $TiO_x/TiON/TiO_x$ cell strongly depend on the thickness of the top and bottom TiO_x oxide layers. As shown in Figure 3b, an increase in the TiO_x oxide thickness from 5 nm to 30 nm gives rise to increased operating voltages for CRS and leads to decreased current levels. It is also suggested that the off-state resistance of the CRS cell increases with an increase in the oxide thickness, as a thicker oxide layer is associated with a higher resistance. In addition, the experimentally observed low set/reset process occurs due to a decrease in the effective bias and the small number of migrated oxygen ions for resistive switching.

A more detailed analysis is currently being conducted to confirm the ability to control additional memory features in our simple triple multilayer cell by varying other parameters, such as the oxygen content and the relative thickness difference between the top/bottom and middle layer. Such findings can hopefully aid in the realization of the CRS characteristics in the near future.

Low- and high-resolution transmission electron microscopy (TEM) images of a hetero TiO_x (5 nm)/TiON (10 nm)/TiO_x (5 nm) triple multilayer junction are shown in **Figure 4**. Low-magnification cross-sectional TEM images (Figure 4a) reveal clear and well-defined interfaces between the TiON and top/bottom TiO_x layers. As expected during the film growth process, the thicknesses of the TiON and TiO_y layers were determined to be 10 nm and 5 nm, respectively. Three distinct Ti oxide-based layers in a layer-by-layer configuration were clearly detected. High-magnification cross-sectional TEM images of a hetero triple junction in an initial (as-grown) state and an "OFF" state after several CRS operations are shown in Figure 4b,c, respectively.

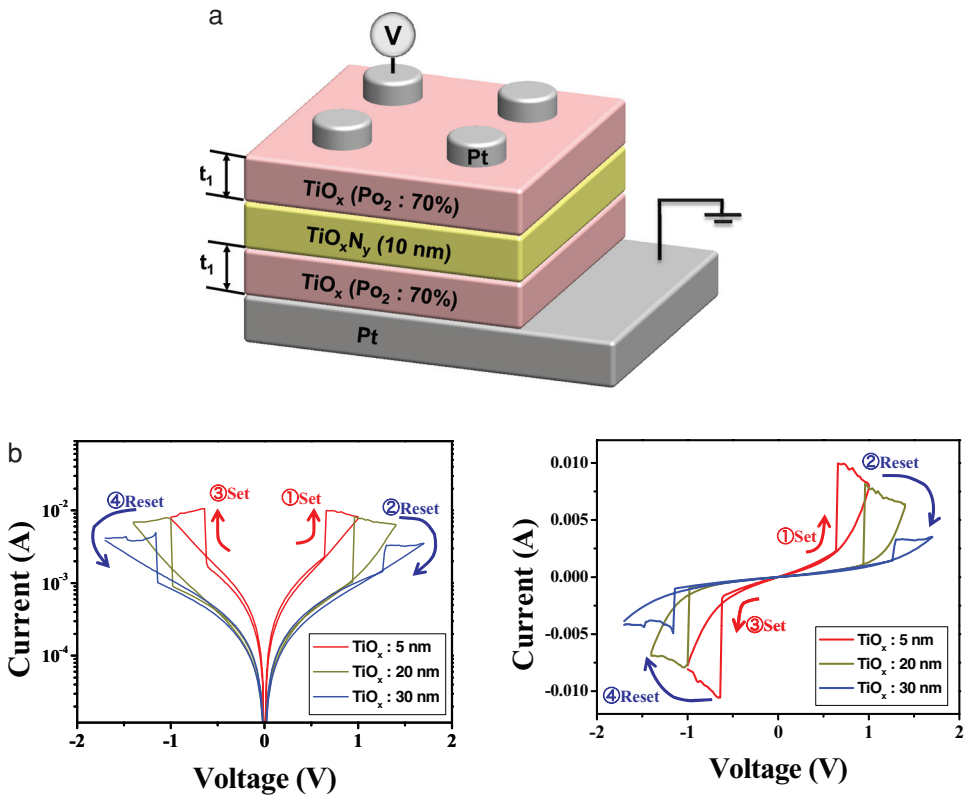

Figure 3. Geometric layout and electrical *I–V* characteristics of hetero Pt/TiO_x/TiON/TiO_x/Pt cells with top and bottom TiO_x layers with different oxygen content and thickness. a) Schematic of the hetero triple multilayer framework with a TiON middle layer. We assume that a redox reaction can be turned on and off in both interfaces of the TiON layer depending on the bias polarity. b) Top and bottom TiO_x oxide thickness dependence of the CRS characteristics at a fixed TiO_x (70%) oxygen content on log (right figure) and linear (left figure) scales. At any given thickness, analogous switching occurs with a similar *I–V* curve shape, but there is a difference in the on-set voltages and current levels. As expected, thinner top and bottom TiO_x layers with a fixed 70% oxygen content cause a variation in the operating threshold voltage.

As illustrated in Figure 4b, certain regions of the top and bottom TiO_x layers are relatively white, suggesting a large amount of oxygen, while the slightly darker color of the middle TiON layer implies a small concentration of oxygen ions. In contrast, in the TEM image of the sample in the "OFF" state after several CRS operations, a relatively white region with a high symmetric distribution across the middle TiON layer is observed at the interfacial regions between the TiON and top/bottom TiO_x layers. Such a finding may indicate a significantly large amount of O^{2-} at the interfacial regions. Therefore, we note that the obtained results

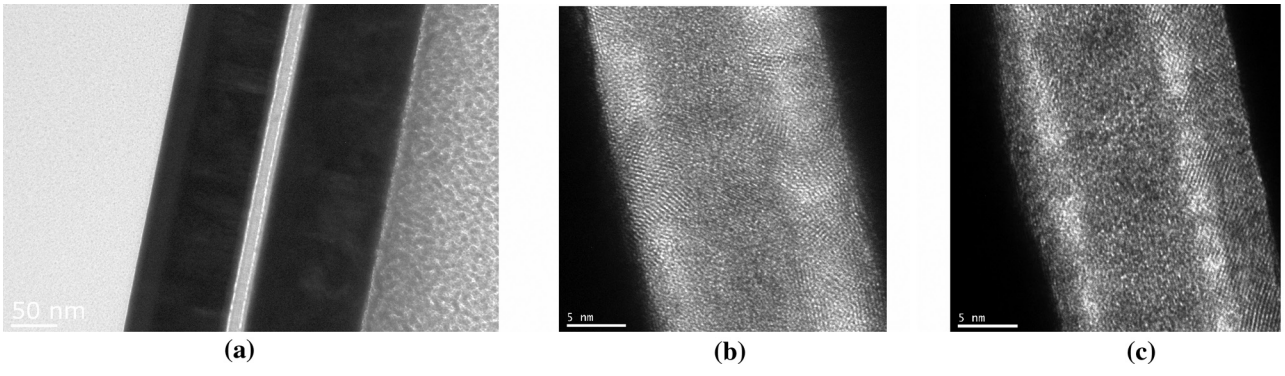

Figure 4. TEM images of a hetero Pt/TiO_x/TiON/TiO_x/Pt cell. a) Low-magnification cross-sectional TEM images of a hetero triple multilayer matrix, where a clear and well-defined interface between two layers can be observed. b) High-magnification cross-sectional TEM images of a hetero triple multilayer matrix in an initial (as-grown) state. The relatively white top and bottom TiO_x layers are indicative of high oxygen content at continuously certain regions, while the slightly darker image indicates low oxygen ion content. c) High-magnification cross-sectional TEM images of a hetero triple multilayer matrix in the ON state. While the middle TiON layer remains unchanged, the relatively white top and bottom TiO_x layers may be stimulated toward a narrow region due to movable oxygen accumulation at the interfaces throughout the conducting channels.

may be related to the movable effect of O^{2-} under a bias. In our previous work on bipolar resistive switching in homo TiO_x/TiO_y structures, depth profile X-ray photoelectron spectroscopy (XPS) measurements of the initial, LRS, and HRS in homo TiO_x/TiO_y structures indicated that bipolar resistive switching behaviors seem to be due to a redox reaction at the interface between the TiO_x and TiO_y.[21] Therefore, the difference between the images of the region adjacent to the TiON layer in the "OFF" state and those captured in the initial state properly reflects different O^{2-} content. More detailed TEM images are being analyzed for a more thorough explanation. Low- and high-resolution TEM images of a homo $TiO_x/TiO_y/TiO_x$ triple multilayer are discussed in Supporting Information (Figure S8).

We next discuss how resistive switching possibly proceeds in a simple all Ti-oxide-based triple geometry. In the scheme described here, we use O^{2-} migration under a bias and the interfacial roles of the top/bottom TiO_x and TiO_y layers. Shown in **Figure 5**a is the initial state of a CRS cell with a top TiO_x layer in the HRS, a middle TiO_y layer in the LRS state, and a bottom TiO_x layer in the HRS. Such a configuration of states arises due to the difference in the oxygen content in the TiO_x and TiO_y layers. Under a bias voltage, each layer in the CRS cell experiences a different voltage drop depending on its resistance. Therefore, the application of a negative first forming bias allows the bottom TiO_x layer to switch to the LRS by producing strong filamentary paths. This is followed by a positive second forming bias that gives rise to other filamentary paths in the top TiO_x layer (Figure 5c). During two step forming process, the middle TiO_y layer with naturally formed leakage paths during growth acted just like a middle electrode and this TiO_y layer was not influenced by the forming processes. After the two-step forming process, all layers in the CRS cell are in the LRS and the total resistance of the CRS cell is in the "ON" state (memristor 1: LRS, memristor 2: LRS), i.e., LRS/LRS holds after the two-step forming process. The CRS operation must then undergo a first reset process (Figure 5d). The O^{2-} ions in the top TiO_x layer drift toward the interface of the TiO_y and are oxidized so as to break the filamentary paths at the interfacial regions between the top TiO_x and middle TiO_y layers. The ruptured filaments at the interfaces permit memristor 1 to return

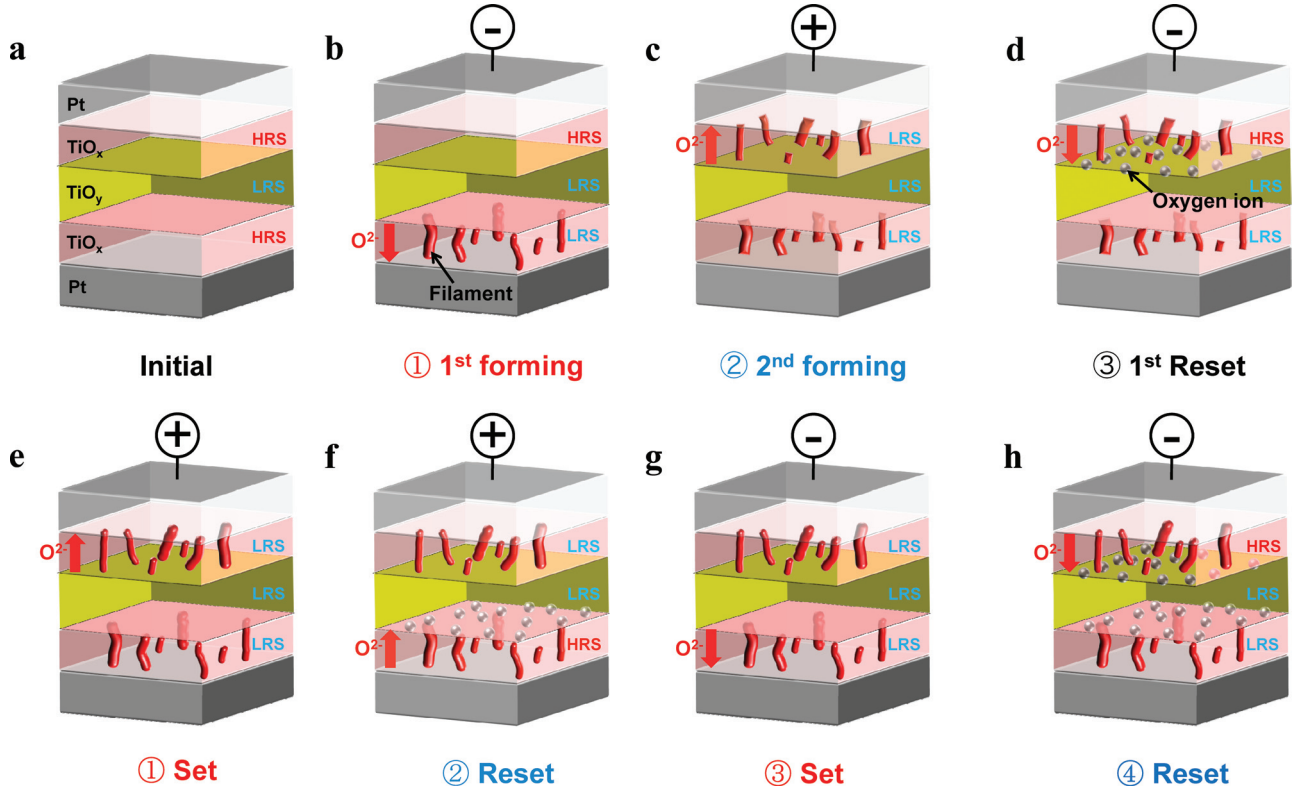

Figure 5. Possible resistive switching models for the CRS behavior in a homo $Pt/TiO_x/TiO_y/TiO_x/Pt$ framework. In our switching model, electrically induced oxygen ion movement at the interfaces between the top/bottom TiO_x and middle TiO_y layers is proposed; O^{2-} and thick stick denote movable oxygen ions and conducting paths (filaments) under a bias. a) Schematic of a CRS cell in the initial state where the TiO_y and TiO_x layers are supposed to have a large (conducting state) and relatively low concentration of oxygen vacancies (insulating state), respectively. b) Schematic of a CRS cell after the first forming process, where the formation of a conducting path is induced in the insulating bottom TiO_x layer due to oxygen ion migration under a bias. c) Schematic of a CRS cell after the second forming process, where inducing a low resistance in the top TiO_x layer drives the CRS cell to switch to the LRS. c,d) Schematics of a CRS cell after the first reset and first CRS set, respectively; resistive switching takes place in switching elements 1 and 2, respectively. e,f) Schematics of a CRS cell after the second CRS reset and third CRS set, respectively; resistive switching occurs in switching elements 2 and 1, respectively. g) Schematic of a CRS cell after the fourth CRS reset, where the CRS cell returns to the state shown in (e). h) Schematic of a CRS cell after the 1^{th} CRS reset, where the CRS cell returns to the state shown in (d).

to the HRS. The total resistance state of the CRS cell becomes a "0" state (HRS/LRS). When a positive bias is applied to the CRS cells (Figure 5e) after the first reset process, most of the voltage drops across memristor 1, which is in the HRS. This permits memristor 1 to switch to the LRS again by driving the migration of O^{2-} to the top electrode, i.e., a redox reaction takes place in this step and re-forms the conducting filament paths. Maintaining a bias allows memristor 2 to switch to the HRS (Figure 5f), that is, a process opposite to the first reset process in memristor 1 occurs. At this moment, the resistance of the CRS cell is in the "1" state (LRS/HRS). The "1" state of the CRS cell switches to the "ON" state (Figure 5g) due to the movement of O^{2-} toward the bottom electrode with an applied negative bias. In addition, the filamentary paths in the bottom TiO_x layer are reformed because most of the effective bias is induced in the bottom TiO_x layer, which is in the HRS. Again, a continuous negative bias permits memristor 1 to switch to the HRS (Figure 5h), similar to the first reset process, and the CRS cell goes backs to the "0" state. Therefore, for CRS operation in a homo triple $TiO_x/TiO_y/TiO_x$ structure, the repeated set/reset behaviors (denoted as ① Set/ ② Reset and ③ Set/ ④ Reset) from Figure 5e–h and the redox reaction due to the in-and-out movement of O^{2-} at interfacial regions leads to a unique CRS butterfly *I–V* curve. Similarly, in a hetero triple $TiO_x/TiON/TiO_x$ structure, the switching mechanism would exhibit the same tendency with relatively low LRS/HRS and HRS/LRS current levels. A decrease in the current levels would be associated with a different response in the interfacial region between the TiON and TiO_x layers, where the TiON layer would generate a relatively weak filamentary path or partially act as an O^{2-} diffusion barrier.[22] Therefore, the population of O^{2-} ions participating in resistive switching at the interfacial regions may be smaller than that in the $TiO_x/TiO_y/TiO_x$ structure (Supporting Information Figure S9). In our triple multilayer cell, a middle metallic electrode is not used for CRS. In addition, our middle TiO_y and TiON layers are relatively conducting with a small amount of O^{2-} so that the proper choice of a highly conducting oxide layer may be sufficient for both CRS and cost-effect scalability if the O^{2-} content can be controlled during growth. Some attempts to develop selection-device-free resistive switching devices[15–18] were recently presented. As such, our proposed model can give reasonable insight into the physical parameters involved in many resistive switching phenomena. However, the device parameters for our triple multilayer structure must be fully explored and optimized in future research.

3. Conclusions

We presented novel device architectures utilizing simple $TiO_x/TiO_y/TiO_x$ and $TiO_x/TiON/TiO_x$ cells as an alternative solution for possible sneak-path disadvantages in future nanoscaled crossbar memory arrays. In particular, additional resistors for the sufficient CRS operation memory margin and conductive middle electrodes for cost-effective scalability were eliminated. Our novel ReRAM geometry would provide promising possibility of the realization of highly integrated 3D non-volatile applications in near future. The origin of the CRS characteristics seems to be attributable to the combined effects of redox reactions at the interfaces between the TiO_y or TiON middle layer and the formation of a conducting path at both the top and bottom TiO_x layers. In addition, it is expected that the nature of this interfacial localized resistive switching will allow for the possible realization of a significantly minimized cell structure. The control of memory windows with different oxygen content in each switching element is promising for diode-free resistive switching devices. However, proper middle oxide materials in oxide-based triple homo and hetero geometries should be chosen so as to establish sufficient memory features. In addition, the switching current, speed, endurance, and retention of novel device architectures must be addressed so that such structures can compete with currently popular silicon-based memory devices, together with densely nanoscale sized reduction cross-bar arrays.

4. Experimental Section

Simple homo TiO_x (top)/TiO_y (middle)/TiO_x (bottom) triple multilayer cells were prepared on a bottom Pt electrode for CRS. Si/SiO_2 substrates were cleaned using a standard oxide wafer cleaning procedure. A 15-nm-thick Ta buffer layer was then prepared on top of the SiO_2/Si substrates, followed by the DC sputtering deposition of a 50-nm-thick Pt bottom electrode at RT. Next, a 5- to 20-nm-thick bottom TiO_x oxygen-rich layer was grown on the Pt bottom electrode using the radio frequency (RF) sputtering technique with a TiO_2 ceramic target in a mixed Ar and oxygen atmosphere. A middle TiO_y layer was grown on the bottom TiO_x layer through RF sputtering in an Ar atmosphere. Finally, a top TiO_x layer was deposited at the same conditions as those used for the bottom TiO_x layer. For defining the junction area, a circular top Pt electrode with a thickness of 100 nm was grown using a metal shadow mask. In order to evaluate the role of different oxygen content in the CRS process, two test devices were fabricated at different oxygen partial pressures (40% and 70% oxygen partial pressure with respect to the total working pressure) so as to generate top and bottom TiO_x layers with different oxygen concentrations.

In the case of a hetero TiO_x (top)/TiON (middle)/TiO_x (bottom) triple multilayer cell, a method similar to that described above was employed. A 100 nm Pt bottom electrode layer was first grown on $Si/SiO_2/Ta$ substrates via DC sputtering. Top and bottom TiO_x layers with thicknesses in the range of 5 nm to 30 nm were then grown by RF magnetron sputtering. As mentioned above, the ratio of O_2 partial pressure to the total pressure was maintained at 70%. A 10-nm-thick TiO_xN_y middle layer was deposited via RF reactive magnetron sputtering using a Ti metal target at RT; the working gas was a mixture of Ar (8 sccm), N_2 (2.5 sccm), and O_2 (0.9 sccm). An extremely small amount of oxygen gas (minimum of 0.9 sccm) was allowed into the system so as to produce a conductive TiON layer. The resistivity of the TiON layer was about 3.9 Ω cm. Finally, 100-nm-thick Pt top electrodes with a diameter of 100 μm were fabricated by DC sputtering using a shadow mask. Electrical measurements were performed with a Keithley 4200 semiconductor parameter analyzer at RT. For the TEM imaging, all cross cutting samples were prepared on a copper grid with a focused ion beam (FIB).

Supporting Information

Supporting Information is available from the Wiley Online Library or from the author.

Acknowledgements

This work was supported by R&D Program of the Ministry of Knowledge Economy and by Leading Foreign Research Institute Recruitment

Program through the National Research Foundation of Korea (NRF) funded by the Ministry of Education, Science and Technology (MEST) (No.2011-00125).

Received: October 2, 2011
Published online: December 21, 2011

[1] R. Waser, Aono, *Nat. Mater.* **2007**, *6*, 833.
[2] The International Technology Roadmap for Semiconductors: 2007 Edition-Emerging Research Devices (ITRS, 2007)
[3] A. Sawa, *Mater. Today* **2008**, *11*, 28.
[4] C. Yoshida, K. Tsunoda, H. Noshiro, Y. Sugiyama, *Appl. Phys. Lett.* **2007**, *91*, 223510.
[5] I. G. Baek, D. C. Kim, M. J. Lee, H.-J. Kim, E. K. Yim, M. S. Lee, J. E. Lee, S. E. Ahn, S. Seo, J. H. Lee, J. C. Park, Y. K. Cha, S. O. Park, H. S. Kim, I. K. Yoo, U.-I. Chung, J. T. Moon, B. I. Ryu, *IEEE Int. Electron Dev. Meet. Tech. Dig.* **2005**, *05*, 750.
[6] A. Flocke, T. G. Noll, C. Kugeler, C. Nauenheim, R. Waser, *8th IEEE Conf. Nanotechnol.* **2008**, *08*, 319.
[7] Q. Xia, J. J. Yang, W. Wu, X. Li, R. S. Williams, *Nano Lett.* **2010**, *10*, 2909.
[8] J. J. Yang, M. D. Pickett, X. Li, D. A. A. Ohlberg, D. R. Stewart, R. S. Williams, *Nat. Nanotechnol.* **2008**, *3*, 429.
[9] J. Liang, H.-S. P. Wong, *IEEE Trans. Electron Dev.* **2010**, *57*, 2531.
[10] S. Yamamoto, Y. Shuto, S. Sugahara, *Jpn. J. Appl. Phys.* **2010**, *49*, 040209.
[11] M. J. Lee, S. I. Kim, C. B. Lee, H. X. Yin, S. E. Ahn, B. S. Kang, K. H. Kim, J. C. Park, C. J. Kim, I. Song, S. W. Kim, G. Stefanovich, J. H. Lee, S. J. Chung, Y. H. Kim, Y. Park, *Adv. Funct. Mater.* **2009**, *19*, 1587.
[12] B. S. Kang, S. E. Ahn, M. J. Lee, G. Steftinovich, K. H. Kim, W. X. Xianyu, C. B. Lee, Y. Park, I. G. Baek, B. H. Park, *Adv. Mater.* **2008**, *20*, 3066.
[13] X. A. Tran, H. Y. Yu, Y. C. Yeo, L. Wu, W. J. Liu, Z. R. Wang, Z. Fang, K. L. Pey, X. W. Sun, A. Y. Du, B. Y. Nguyen, M. F. Li, *IEEE Electron Dev. Lett.* **2011**, *32*, 396.
[14] D. S. Golubović, A. H. Miranda, N. Akil, R. T. F. van Schaijk, M. J. van Duuren, *Microelectron. Eng.* **2007**, *84*, 2921.
[15] E. Linn, R. Rosezin, C. Kugeler, R. Waser, *Nat. Mater.* **2010**, *9*, 403.
[16] R. Rosezin, E. Linn, L. Nielen, C. Kugeler, R. Bruchhaus, R. Waser, *IEEE Electron Dev. Lett.* **2011**, *32*, 191.
[17] S. M. Yu, J. L. Liang, Y. Wu, H.-S. P. Wong, *Nanotechnology* **2010**, *21*, 465202.
[18] M. J. Lee, C. B. Lee, D. Lee, S. R. Lee, M. Chang, J. H. Hur, Y. B. Kim, C. J. Kim, D. H. Seo, S. Seo, U. I. Chung, I. K. Yoo, K. Kim, *Nat. Mater.* **2011**, *10*, 625.
[19] C. Nauenheim, C. Kuegeler, A. Ruediger, R. Waser, *Appl. Phys. Lett.* **2010**, *96*, 122902.
[20] Y. H. Do, J. S. Kwak, Y. C. Bae, K. H. Jung, H. S. Im, J. P. Hong, *Appl. Phys. Lett.* **2009**, *95*, 093507.
[21] Y. C. Bae, A. R. Lee, J. S. Kwak, H. S. Im, Y. H. Do, J. P. Hong, *Appl. Phys. A* **2011**, *102*, 1009.
[22] J. S. Kwak, Y. H. Do, Y. C. Bae, H. S. Im, J. H. Yoo, M. G. Sung, Y. T. Hwang, J. P. Hong, *Appl. Phys. Lett.* **2010**, *96*, 223502.
[23] Y. H. Do, J. S. Kwak, Y. C. Bae, J. H. Lee, Y. Kim, H. S. Im, J. P. Hong, *Curr. Appl. Phys.* **2010**, *10*, E71.
[24] Y. H. Do, J. S. Kwak, Y. C. Bae, K. Jung, H. S. Im, J. P. Hong, *Thin Solid Films* **2010**, *518*, 4408.